

Edge-disorder-dependent transport length scales in graphene nanoribbons: From Klein defects to the superlattice limit

Alessandro Cresti^{1,2} and Stephan Roche^{2,3}¹CEA, LETI, MINATEC, F38054 Grenoble, France²Institute for Nanoscience and Cryogenics INAC/SP2M/L_Sim, CEA, 17 rue des Martyrs, 38054 Grenoble Cedex 9, France³Institute for Materials Science, TU Dresden, D-01062 Dresden, Germany

(Received 3 April 2009; published 16 June 2009)

We report a numerical study of quantum transport in zigzag graphene nanoribbons with varying edge-disorder profile. The transport length scales, such as the elastic mean-free paths and the localization lengths, are shown to fluctuate by orders of magnitude depending on the topology of edge irregularities as well as their correlation degree. This might result in considerable sample-to-sample fluctuations of the corresponding transport gap, whose occurrence has been recently discussed both experimentally and theoretically.

DOI: [10.1103/PhysRevB.79.233404](https://doi.org/10.1103/PhysRevB.79.233404)

PACS number(s): 73.21.-b, 73.22.-f, 73.63.-b, 81.05.Uw

Two-dimensional graphene is a newly discovered carbon-based material with spectacular electronic and transport properties.¹ Additionally, the active search for its wafer scale integration is driven by the technological interest for a beyond complementary metal-oxide semiconductor nanoelectronics.² Graphene nanoribbons (GNRs) are strips of graphene with width varying from a few to several tens of nanometers, depending on their fabrication processes.³ In contrast to two-dimensional graphene which is a zero-gap semiconductor, the narrow lateral size of GNRs entails quantum confinement effects and allows a modulation of the corresponding electronic band gap. Two types of GNRs with highly symmetric edges (zigzag and armchair) have been predicted⁴ and experimentally observed. Nonetheless, experimental characterization with Raman studies,⁵ scanning tunneling microscopy (STM),⁶ or high-resolution electronic transmission microscopy⁷ has revealed a large spectrum of topologically different edge defects [such as the Klein defect observed by STM (Ref. 6)]. Large fluctuations of low-temperature conductance have been reported in the Coulomb blockade regime,⁸ and the occurrence of a transport gap driven by edge-disorder-induced localization effects has been debated theoretically.⁹⁻¹⁴ However, the considerable topological richness of edge defects observed experimentally^{6,7} clearly demands for a more in-depth exploration of their consequence on GNRs transport properties.

In this Brief Report, we report a deep correlation between transport properties and topological features of edge disorder. In relation to experimental observations, we explore the impact of specific edge imperfections such as Klein defects or missing hexagons, with varying spacing and density, on quantum conduction regimes. By defining a general criterion for characterizing the disordered edge defect density, charge transport properties for different types of topological disorder can be more quantitatively contrasted. To compute transport properties, we make use of the Green's function computational method adapted to a first-nearest-neighbor description of the GNRs.¹⁵ This enables the identification of the conduction regime (ballistic, diffusive, or localized) and a direct calculation of the related scaling lengths (elastic mean-free path ℓ_e and localization length ξ). Several types of model disorders have already been studied by such a tech-

nique in the literature (see Ref. 16 for a review). Here, elastic mean-free paths and localization lengths are extracted numerically from the length scaling analysis of the quantum conductance by considering that, according to the considered regimes, $\bar{T} = N_{\perp} / (1 + L/\ell_e)$ or $\ln \bar{T} \propto -L/\xi$, where T is the transmission coefficient of the system, L is the length, N_{\perp} is the number of active conduction channels, and the overbar indicates the average over different samples. Both quantities are energy dependent and strongly vary as a function not only of the local nature of the underlying disorder, but also of the GNR width and symmetry, which determine the subbands profile.

Following Ref. 4, we refer to a zigzag (armchair) graphene nanoribbons composed of N zigzag (dimers) chains as N -zGNR (N -aGNR). A debated issue is the possible higher robustness of zGNR conductance with respect to aGNR for a similar defect density.^{9,10} Here we focus on zGNRs and investigate the effect of given local edge defect topology and density. To describe the ribbon energetics, we adopt a standard one-orbital-per-site tight-binding Hamiltonian with zero on-site energy and $t = -2.7$ eV hopping parameter.¹

To give an idea of the impact of edge disorder, we start by considering the conductance properties of 16-zGNRs with length $L = 500$ nm and randomly removed carbons on their edges with an equal probability of 7.5% but varying the allowed nature of edge imperfections (Fig. 1). Figure 1(a) corresponds to the case with the highest complexity for the disorder profile, where dangling edge atoms (defect D1), one (defect D2), two (defect D3), or more missing hexagons defects coexist. Then, the disorder complexity is reduced by disallowing specific types of local defects in the disorder profile. Three edge-disorder profiles are compared and yield strikingly different results. Figure 1(a) shows the conductance as a function of the energy E of the injected electrons for the 16-zGNR with the highest level of defect complexity. The transmission turns out to be mostly suppressed within the first plateau (region marked by two vertical lines close to $E = 0$, where only one conductive channel is active), thus indicating that the electronic system is already mostly in the Anderson regime with a localization length $\xi \leq L$.

Figure 1(b) shows the conductance of a disordered ribbon in which dangling edge atoms (D1) have been removed from

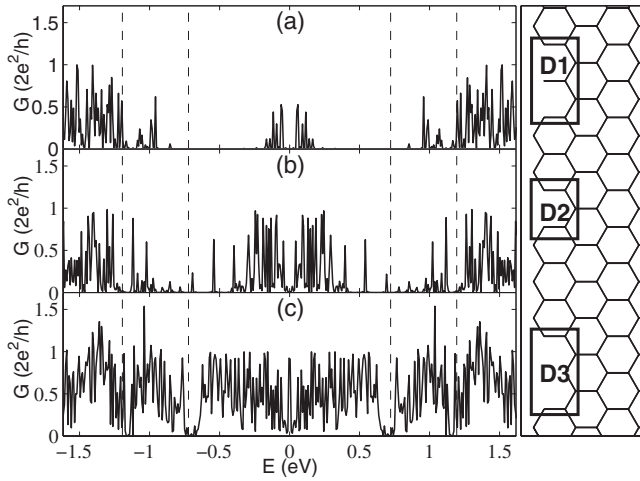


FIG. 1. Left: conductance of a disordered 16 zGNR (with length $L=500$ nm) with 7.5% of randomly removed edge carbon atoms. Case (a) includes dangling atoms defects (D1), single (D2), and double (D3) missing hexagons defects, whereas D1 is disallowed in case (b) and D1 and D2 are disallowed for case (c). Right: schematic representation of the edge disordered ribbon with D1, D2, and D3 defects shown in boxes.

the disorder profile. In comparison with the prior pattern, the new resulting conductance is significantly enhanced in the first plateau, although some regions of the spectrum remain vanishingly conductive. Finally, by removing the possibility of both dangling edge atoms and single missing hexagons (D1 and D2), the ribbon shows a stronger robustness against disorder. This is clearly seen in Fig. 1(c), where the conductance keeps a value close to $G_0=2e^2/h$, as obtained in the clean GNR for a ballistic regime.¹⁷ In conclusion, the conductance ranges from a localized to a quasiballistic regime depending on the degree of defect complexity and ribbon length.

The previous considerations highlight the importance of investigating the impact of different types of defects on the transport properties of GNRs since the level of complexity of the disorder itself plays a key role. In the following, we consider four different types of defect randomly distributed along the edges of the ribbon: Klein defects (i.e., dangling carbon atoms linked to the edges), single missing hexagons (with at least one hexagon between two adjacent defects), two consecutive missing hexagons (with at least two hexagons between two adjacent defects), and three consecutive missing hexagons (with at least three hexagons between two adjacent defects). The degree of disorder in each case is determined by the probability P , which fixes (within a precision of 2%) the number of defects on each edge to $P \times L/a$, where $a=2.46$ Å is the lattice parameter. To build the edge-disorder profile, we start from a pristine zGNR and remove the carbons on the edges randomly, as in the case of Fig. 1, but taking into account the constraints related to the different defect topologies under investigation. In this process, the probability of removing atoms is not P , but it is chosen in such a way that the total number of defects (and not the total number of removed carbons) is proportional to P . This allows us to contrast transport properties for different defect types and comparable disorder degree.

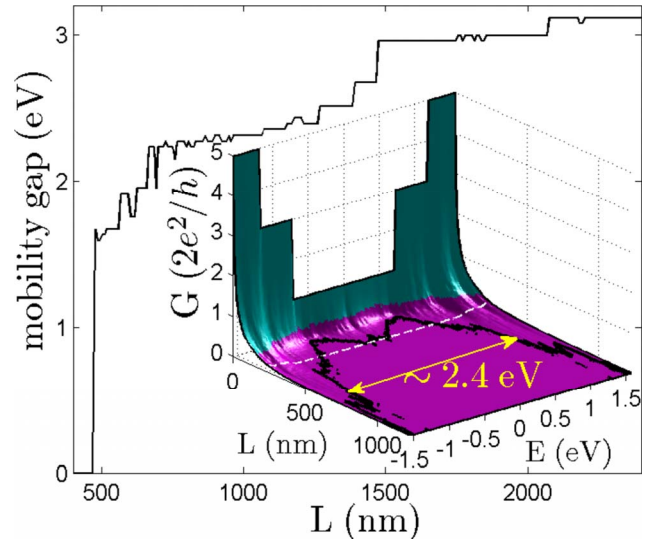


FIG. 2. (Color online) Main frame: transport gap as a function of L . Inset: average conductance (1000 different configurations) of disordered 16 zGNR (defects are single missing hexagons with density $P=7.5\%$). The bold line marks the (L, E) region for which $G < 0.01 \times 2e^2/h$. The L dependence of the transport gap width is defined starting from $L \geq 470$ nm (dashed line). A particular value is shown (double arrow line) at $L=1250$ nm.

In the inset of Fig. 2, we show the average conductance $G = \bar{T}(2e^2/h)$, where \bar{T} is the average transmission coefficient, as a function of the electron energy E and the length of the system L , in the case of a 16-zGNR with edge defect only constituted of single missing hexagons distributed with a probability $P=7.5\%$. The average is performed over an ensemble of 1000 different configurations. The quantized conductance pattern of pristine GNRs sets the limit at $L=0$. When L increases, the system first enters the diffusive regime, where the conductance decays linearly with length before entering the localization regime where the conductance decreases exponentially (Fig. 2). To discriminate between the diffusive and the localization regime, we use the criterion defined in Ref. 18 and relate it to the values of $\Delta(T)/\bar{T}$ and $\Delta(\ln T)/\ln T$ (Δ stands for the standard deviation). We have thus the elements to extract the mean-free path ℓ_e and the localization length ξ from the transmission coefficients. From the average conductance, it is further possible to estimate some *transport gap* of the GNR according to the general criterion adopted by Evaldsson *et al.*,¹¹ which identifies the gap as the energy region where $G < 0.01 \times 2e^2/h$ (also adopted by experiments³). For the considered edge-disorder profile, such criterion is fulfilled when $L \geq 470$ nm. The transport gap is further enlarged with increasing the ribbon length, owing to the increasingly stronger contribution of backscattering and quantum interference effects.

The understanding of conductance scaling in such systems is further deepened by performing an extensive analysis of transport length scales for the four different types of disorder considered here and schematically reported in the insets of Fig. 3. For each of the four types of defect, we consider density probabilities $P=2.5\%$, 5% , and 7.5% and compare the results for the mean-free path ℓ_e in Fig. 3.

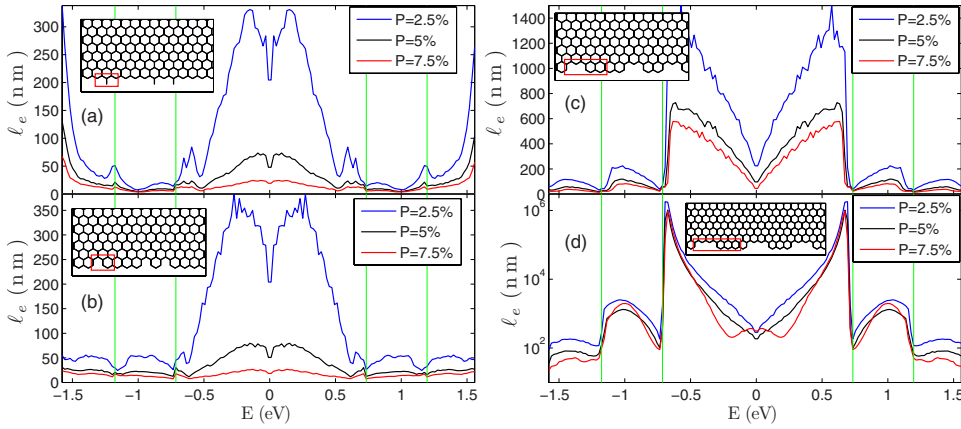


FIG. 3. (Color online) Mean-free path for a 16 zGNR with (a) $P=2.5\%$, 5% , and 7.5% of Klein defects, (b) single missing hexagon defects, (c) two missing hexagons defects, and (d) three missing hexagons defects. Vertical lines show onsets of new subbands.

The case of Klein defects is reported in Fig. 3(a), where ℓ_e shows important fluctuations with a much more robust ballistic regime up to ~ 200 nm for energies close to the charge neutrality point (CNP) and at the considered defect densities. Scattering probability is strongly enhanced in the higher subbands, as already found for other models of disorder.¹⁶ The mean-free path decays with increasing defect density, although the scaling law deviates from a pure linear behavior. The cases of single missing hexagon defects, two missing hexagons defects, and three missing hexagons defects are reported in Figs. 3(b)–3(d), respectively. The mean-free path patterns are found to strongly depend on the defect type, with variations of up to 5 orders of magnitude. In particular, for the chosen density P , short-range defects [as Klein defects or single missing hexagons defects of Figs. 3(a) and 3(b)] yield mean-free paths considerably shorter in contrast to more long-range defects [two or three missing hexagons defects of Figs. 3(c) and 3(d)]. More regular long-range defects entail the presence of regular regions with a pristine structure that has a reduced impact on the transport properties of the system. Even a small difference in the defect topology leads to considerable differences in the scaling lengths, as in the case of one missing hexagon defects $\ell_e < 375$ nm in the first plateau, and in the case of two missing hexagons defects ℓ_e goes up to 1450 nm in the same energy window. In the case of three missing hexagons defects, this effect is even stronger and the mean-free path reaches values on the order of 10^6 nm in the first plateau, as clearly visible in Fig. 3(d). By looking carefully at Fig. 3(d), we notice that $\ell_e^{7.5\%} > \ell_e^{5\%}$ in certain regions of energy corresponding to one or three active conduction channels. This observation, which might sound counterintuitive at a first sight, sheds light on the other factor that contributes to the decrease in disorder effects: spatial correlation. When increasing their length and density, defects are forced to organize into more and more spatially correlated structures and tend progressively to a “superlattice” profile. The presence of regular patterns with energy structure close to that of periodic systems lowers backscattering efficiency and the ratio between the number of localized and delocalized states for a given system length and charge-carrier energy. The long ℓ_e observed when only one conductive channel is active and for all the four considered cases is attributable to the fact that, in this energy region, currents mainly flow through the bulk, far from the

irregular edges.¹⁹ This is also true for region very close to the CNP, where the states are mainly located at the edges but current flowing along the edges is prevented by the absence, in the model, of coupling between carbon atoms belonging to the same sublattice. A more realistic two or three nearest-neighbor tight-binding description would probably affect the results around the CNP.¹² When comparing Figs. 3(a) and 3(b), we also notice that close to the CNP ℓ_e is almost the same for Klein defects and single missing hexagon defects. This peculiarity can be understood by considering that, in order to evaluate the Green’s functions, the extra carbon acts on the linked edge atom by means of the self-energy $\Sigma = t^2/(E + \eta)$, where an infinitesimal imaginary part η is included into the energy. When the energy is very close to the CNP, Σ diverges thus preventing electrons to occupy the corresponding site on the edge. As a consequence, in this energy range, the two types of disorder are completely equivalent.

An analogous study on the localization lengths ξ gives consistent results. In this respect, it is interesting to compare the ratio ξ/ℓ_e , for chosen defect type and density, and the number of active conduction channels N_\perp in the ballistic regime. In Fig. 4, we report this ratio for single missing hexagon and two missing hexagons types of disorder with $P=5\%$. It is found that $\xi/\ell_e \sim N_\perp$, which is in agreement

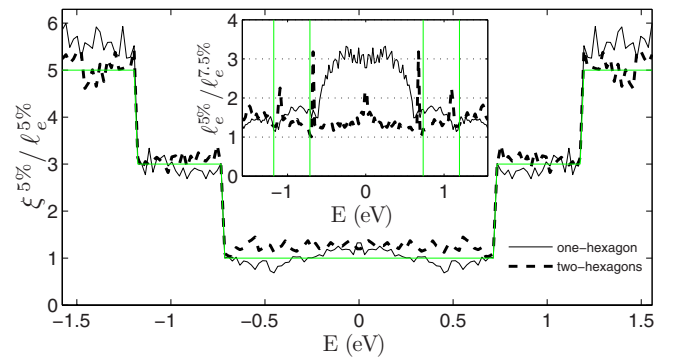


FIG. 4. (Color online) Main frame: $\xi^{5\%}/\ell_e^{5\%}$ for disorder profiles constituted of single missing hexagons and two missing hexagons with $P=5\%$. The steplike curve indicates the number of active conduction channels. Inset: $\ell_e^{5\%}/\ell_e^{7.5\%}$ for the same situation. Vertical lines show onsets of new subbands.

with the so-called Thouless relation, crosslinking such fundamental transport length scales, although the exact scaling factor is only well controlled for a single channel or in the limit of large channel number.¹⁸

A further analysis can be performed on the scaling behavior of ℓ_e as a function of the defect density P and for chosen type of defect. As an example, the inset of Fig. 4 reports the ratio $\ell_e^{5\%}/\ell_e^{7.5\%}$ for the disorder constituted of single missing hexagons and two missing hexagons. In both cases, when a few conduction channels are active, the ratio fluctuates around different values, especially for the shorter-range disorder, while at higher energies it is closer to the value $7.5/5=1.5$. This behavior, which is also observed for different values of P and disorder types, indicates that $\ell_e \sim P^{-1}$ when the energy is far enough from the CNP (and the wave function is more uniformly distributed along the ribbon sec-

tion), while there is no well-defined scaling law around the $E=0$.

In conclusion, the impact of defect topology on the transport properties of zGNRs has been explored. Specific effects of each type of defect have allowed us to unveil physical behaviors otherwise buried under the complexity of more general theoretical models or experimental samples. Strong variations in transport length scales were found to depend on the nature of the defects through their spatial extension and correlation. This should have some consequences on the transport gaps and could be at the origin of large sample-to-sample low-temperature conductance fluctuations.

A.C. acknowledges support from CARNOT graphene from LETI, while S.R. is indebted to the Alexander Von Humboldt Foundation for financial support.

-
- ¹A. H. Castro Neto, F. Guinea, N. M. R. Peres, K. S. Novoselov, and A. K. Geim, *Rev. Mod. Phys.* **81**, 109 (2009).
- ²C. Berger, Z. Song, X. Li, X. Wu, N. Brown, C. Naud, D. Mayou, T. Li, J. Hass, A. N. Marchenkov, E. H. Conrad, P. N. First, and W. A. de Heer, *Science* **312**, 1191 (2006).
- ³M. C. Lemme, T. J. Echtermeyer, M. Baus, and H. Kurz, *IEEE Electron Device Lett.* **28**, 282 (2007); Z. Chen, Y.-M. Lin, M. J. Rooks, and Ph. Avouris, *Physica E (Amsterdam)* **40**, 228 (2007); M. Y. Han, B. Ozyilmaz, Y. Zhang, and Ph. Kim, *Phys. Rev. Lett.* **98**, 206805 (2007); X. Li, X. Wang, L. Zhang, S. Lee, and H. Dai, *Science* **319**, 1229 (2008); X. Wang, Y. Ouyang, X. Li, H. Wang, J. Guo, and H. Dai, *Phys. Rev. Lett.* **100**, 206803 (2008); Y.-M. Lin, V. Perebeinos, Z. Chen, and Ph. Avouris, *Phys. Rev. B* **78**, 161409(R) (2008).
- ⁴K. Nakada, M. Fujita, G. Dresselhaus, and M. S. Dresselhaus, *Phys. Rev. B* **54**, 17954 (1996); K. Wakabayashi, *ibid.* **64**, 125428 (2001); K. Sasaki, S. Saito, and R. Saito, *Appl. Phys. Lett.* **88**, 113110 (2006).
- ⁵L. G. Cançado, M. A. Pimenta, B. R. A. Neves, M. S. S. Dantas, and A. Jorio, *Phys. Rev. Lett.* **93**, 247401 (2004); C. Casiraghi, A. Hartschuh, H. Qian, S. Piscanec, C. Georgi, A. Fasoli, K. S. Novoselov, D. M. Basko, and A. C. Ferrari, *Nano Lett.* **9**, 1433 (2009).
- ⁶Y. Niimi, T. Matsui, H. Kambara, K. Tagami, M. Tsukada, and H. Fukuyama, *Phys. Rev. B* **73**, 085421 (2006); Y. Kobayashi, K. I. Fukui, T. Enoki, and K. Kusakabe, *ibid.* **73**, 125415 (2006).
- ⁷Z. Liu, K. Suenaga, P. J. F. Harris, and S. Iijima, *Phys. Rev. Lett.* **102**, 015501 (2009); Ç. Ö. Girit, J. C. Meyer, R. Erni, M. D. Rossell, C. Kisielowski, L. Yang, C.-H. Park, M. F. Crommie, M. L. Cohen, S. G. Louie, and A. Zettl, *Science* **323**, 1705 (2009); J. C. Meyer, C. Kisielowski, R. Erni, M. D. Rossell, M. F. Crommie, and A. Zettl, *Nano Lett.* **8**, 3582 (2008); X. Jia, M. Hofmann, V. Meunier, B. G. Sumpter, J. Campos-Delgado, J. M. Romo-Herrera, H. Son, Y.-P. Hsieh, A. Reina, J. Kong, M. Terrones, and M. S. Dresselhaus, *Science* **323**, 1701 (2009).
- ⁸C. Stampfer, J. Güttinger, S. Hellmüller, F. Molitor, K. Ensslin, and T. Ihn, *Phys. Rev. Lett.* **102**, 056403 (2009); F. Molitor, A. Jacobsen, C. Stampfer, J. Güttinger, T. Ihn, and K. Ensslin, *Phys. Rev. B* **79**, 075426 (2009); H. Miyazaki, S. Odaka, T. Sato, S. Tanaka, H. Goto, A. Kanda, K. Tsukagoshi, Y. Ootuka, and Y. Aoyagi, *Appl. Phys. Express* **1**, 024001 (2008); X. Liu, J. Oostinga, A. Morpurgo, and L. Vandersypen, arXiv:0812.4038 (unpublished); K. A. Ritter and J. W. Lyding, *Nature Mater.* **8**, 235 (2009).
- ⁹D. A. Areshkin, D. Gunlycke, and C. T. White, *Nano Lett.* **7**, 204 (2007); D. Gunlycke, D. A. Areshkin, and C. T. White, *Appl. Phys. Lett.* **90**, 142104 (2007); D. Gunlycke and C. T. White, *Phys. Rev. B* **77**, 115116 (2008).
- ¹⁰D. Querlioz, Y. Apertet, A. Valentin, K. Huet, A. Bournel, S. Galdin-Retailleau, and P. Dollfus, *Appl. Phys. Lett.* **92**, 042108 (2008).
- ¹¹M. Evaldsson, I. V. Zozoulenko, H. Xu, and T. Heinzel, *Phys. Rev. B* **78**, 161407(R) (2008).
- ¹²M. Wimmer, I. Adagideli, S. Berber, D. Tománek, and K. Richter, *Phys. Rev. Lett.* **100**, 177207 (2008).
- ¹³E. R. Mucciolo, A. H. Castro Neto, and C. H. Lewenkopf, *Phys. Rev. B* **79**, 075407 (2009).
- ¹⁴A. R. Akhmerov and C. W. J. Beenakker, *Phys. Rev. B* **77**, 085423 (2008).
- ¹⁵A. Cresti, G. Grosso, and G. Pastori Parravicini, *Phys. Rev. B* **76**, 205433 (2007).
- ¹⁶A. Cresti, N. Nemeč, B. Biel, G. Niebler, F. Triozon, G. Cuniberti, and S. Roche, *Nano Res.* **1**, 361 (2008).
- ¹⁷K. Wakabayashi, M. Fujita, H. Ajiki, and M. Sigrist, *Phys. Rev. B* **59**, 8271 (1999); F. Muñoz-Rojas, D. Jacob, J. Fernández-Rossier, and J. J. Palacios, *ibid.* **74**, 195417 (2006).
- ¹⁸D. J. Thouless, *Phys. Rev. Lett.* **39**, 1167 (1977); C. W. Beenakker, *Rev. Mod. Phys.* **69**, 731 (1997); R. Avriiler, S. Roche, F. Triozon, X. Blase, and S. Latil, *Mod. Phys. Lett. B* **21**, 1955 (2007).
- ¹⁹L. P. Zárbo and B. K. Nikolić, *EPL* **80**, 47001 (2007).